arXiv:2106.08941v1 [eess.SY] 16 Jun 2021

Mean-value exergy modeling of internal combustion engines: characterization of feasible operating regions

Gabriele Pozzato[a], Denise M. Rizzo[b], Simona Onori[a,*]

[a] *Energy Resources Engineering Department, Stanford University, Stanford, CA, 94305 USA*
[b] *U.S. Army CCDC Ground Vehicle Systems Center, 6501 E. 11 Mile Road, Warren, MI 48397*

Abstract

In this paper, a novel mean-value exergy-based modeling framework for internal combustion engines is developed. Starting from a detailed description of the in-cylinder dynamics, the exergy balance is solved for each engine operating point and, for the first time, static maps describing the availability transfer and destruction phenomena as a function of speed and load are derived. The application of the proposed modeling strategy, from the construction of the static maps to their usage, is shown for a military series hybrid electric vehicle. Ultimately, these static maps, while providing insightful information about inefficiencies over the whole operating field of the engine, are the enabling step for the development of exergy-based control strategies aiming at minimizing the overall operational losses of ground vehicles.

1. Introduction

In the quest for sustainability, increasing fuel economy, reducing vehicular emissions, and improving energy efficiency are mandatory actions. To this aim, researchers and companies have joined the efforts, devoting time and resources to the development of new powertrain solutions. In this scenario, military ground vehicles are migrating from standard internal combustion engine (ICE) powertrains to electrified ones [1]. This allows to improve energy efficiency while reducing operational costs and even noise emissions, enabling also stealthier operations. To exploit the full potential of these technologies, formal modeling and analysis techniques must be developed for a complete understanding of the irreversibilities degrading the efficiency of the system and, consequently, for the formulation of "efficiency aware" control and management strategies [2].

In this framework, availability, or exergy, is a useful metric to quantify the thermal, mechanical, and chemical work a system can perform with respect to a reference state, usually called environment. On the contrary to approaches based on the first law of thermodynamics, which assume the conservation of energy, exergy-based modeling implements the second law of thermodynamics introducing the concept of entropy. This allows for the explicit quantification of the irreversibilities of the system and, ultimately, for efficiency improvement.

Exergy-based modeling is a well-known concept in aerospace engineering, where diverse systems must be integrated and balanced to produce effective designs. In [3] and [4], the authors propose an availability analysis for rockets and launch vehicles, respectively. The design and optimization of hypersonic aircrafts is tackled in [5] and [6]. Exergy analysis is applied also in other fields, such as naval engineering [7] and power generation [8, 9]. Moreover, availability concepts are used for the analysis of combustion processes in engines. ICEs are complex systems composed of up to 2000 interacting parts subjected to friction, heat transfer, and thermomechanical stresses. Controlling in-cylinder combustion phenomena is imperative to optimize braking work generation, while minimizing inefficiencies. Considering spark ignition engines, [10] and [11] analyze the exergy transfer and destruction processes in engines fueled with synthetic and natural gas, respectively. For what concerns compression ignition engines, an overview on exergy modeling for both naturally aspirated and turbocharged diesel engines is provided by [12]. In [13, 14] and [15], steady-state and transient operating conditions are analyzed, respectively. The authors of [16] exam-

*corresponding author

ine the availability balance of a diesel engine fueled with different biodiesels. In [17], a similar analysis is performed considering biodiesel, diesel, and bioethanol blends.

On the one hand, exergy-based modeling has been widely used for system design optimization. On the other hand, only a few works show the potential of the approach for the development of "efficiency aware" control algorithms. In [18], [19], and [20], the effectiveness of exergy-based control algorithms is shown for air conditioning systems, ships, and aircrafts, respectively. In the context of ground vehicles' powertrain, [21] successfully optimizes the in-cylinder combustion in homogeneous charge compression ignition (HCCI) engines relying on model predictive control (MPC), allowing for 6.7% fuel saving. The authors of [21] rely on crank-angle resolved engine models, effective for optimization of the combustion process variables (such as spark, injection, and valve timings) but impracticable for the development of powertrain-level management strategies.

The scarcity of exergy-based analysis in the ground vehicles field has spurred the authors to develop a comprehensive exergy-based modeling framework for hybrid and electric vehicles (HEV and EV) [22]. The description is control-oriented and modular and allows for the quantification of inefficiencies in the energy storage and conversion devices of the powertrain – electrochemical energy storage, electric motor, and ICE –. The simplified ICE model employed in [22], while being suitable for powertrain-level quantification of irreversibilities, imposes some limitations, i.e., it does not allow for an explicit characterization of all the feasible operating regions of the engine. Since ICEs are the principal source of irreversibility within hybrid powertrains, the development of a more sophisticated model is mandatory.

In this paper, the overarching research objective is the formulation of a thorough model for exergy quantification in ICEs. The model is mean-value and, given its low computational burden, suitable for control applications and for the development of supervisory management strategies. For the first time, a clear methodology for the derivation of a mean-value exergy-based model for compression ignition diesel engines, accounting for all the transfer and destruction availability phenomena, is defined. In particular, a characterization of combustion irreversibilities, based on the analysis of the chemical potentials, is provided. The outcomes of the approach are static maps describing the exergetic behavior of the engine as a function of speed and load. These maps, which must be computed only once given a certain engine, are the enabling factors for the development of "exergy management strategies", i.e., they provide useful information on the engine efficiency (and inefficiency) for each operating condition and with low computational burden. This information can be used to minimize the operational losses of ground vehicles, e.g., in the framework described in [22]. The approach is here developed starting from a series military HEV, however, the procedure is general and can be used in any device equipped with an ICE.

The remainder of the paper is organized as follows. In Section 2, fundamental concepts related to availability modeling are summarized. Section 3 shows the vehicle technical specifications. In Section 4, the ICE modeling, in terms of airflow path, combustion reaction, and in-cylinder dynamics, is shown. Moreover, the derivation of average in-cylinder pressure, heat transfer, and temperature maps is detailed. Section 5, starting from Section 4, formalizes the exergy-based modeling of the ICE, introducing all the sources of exergy transfer and destruction phenomena. In Section 6, the static maps for each exergy term are built and results over a military driving cycle are shown. Eventually, conclusions are carried out in Section 7.

2. Exergy modeling: definitions

In this section, some fundamental concepts related to exergy modeling are introduced. Also, at the end of the paper, the notation and nomenclature are provided to the reader (page 17).

Definition 2.1 (Exergy)**.** Exergy (or availability) is the maximum useful work that can be extracted from a system at a given state, with respect to a thermodynamic and chemical reference state.

Definition 2.2 (Reference state)**.** The reference state (also referred as dead state or environment) is characterized by a pressure P_0, a temperature T_0, and a mixture of chemical species combined according to the molar fractions f_0. At the reference state, the entropy of the system is maximized and the work availability (chemical, thermodynamical, mechanical, etc.) is zero.

Figure 1: Oshkosh M-ATV [23].

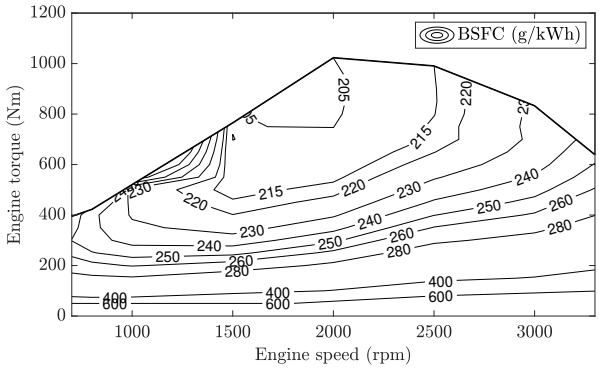

Figure 2: BSFC map.

Definition 2.3 (Restricted state)**.** The restricted state is the condition of a system not in chemical equilibrium with respect to the reference state but at pressure and temperature P_0 and T_0, respectively.

From now on, quantities expressed with respect to the reference and restricted state are denoted by subscript 0 and superscript $\star$, respectively.

3. Vehicle technical specifications

In this work, a mine-resistant ambush-protected all-terrain vehicle (Oshkosh M-ATV) is analyzed (Figure 1). The vehicle is characterized by a series hybrid electric powertrain, comprising of a diesel generator, four 95 kW brushless permanent magnet in-hub motors, and a lithium-ion battery pack. The diesel generator is composed by a Power Stroke 6.4L V8 turbocharged diesel engine (with a peak power of 260 kW at 3000 rpm) [24] and a 265 kW electric generator, which converts the mechanical power into electrical.

Being this research focused on the development of a comprehensive exergy-based model for the ICE, only the parameters for the diesel engine are provided (Table 1). Moreover, the brake-specific fuel consumption (BSFC), retrieved from [25], is shown in Figure 2. Additional details on the powertrain architecture can be found in [26].

Parameter	Unit	Value	Reference
b	(-)	1.4	[27]
c	(-)	$-\log(0.001)$	[28]
d	(-)	2	[29]
$f_{N_2,0}$	(-)	0.7567	[21]
$f_{CO_2,0}$	(-)	0.0003	[21]
$f_{H_2O,0}$	(-)	0.0303	[21]
$f_{O_2,0}$	(-)	0.2035	[21]
$f_{others,0}$	(-)	0.0092	[21]
r_c	(-)	17.5:1	[24]
n_{cyl}	(-)	8	[24]
CN	(-)	50	[30]
x_{EGR}	(-)	0.2 (or 20%)	[31]
x	(-)	14.4	[12]
y	(-)	24.9	[12]
a	(m)	52.5×10^{-3}	[24]
l	(m)	210×10^{-3}	[24]
B	(m)	98.2×10^{-3}	[24]
L	(m)	105×10^{-3}	[24]
$V_{d,tot}$	(l)	6.4	[24]
T_0	(K)	298.15	-
T_I	(K)	323.15	-
T_w	(K)	400	[32]
P_0	(bar)	1	-
P_I	(bar)	1	-
C_1	(kPa)	75	[30]
C_2	(s kPa)	0.458	[30]
C_3	(s^2kPa/m^2)	0.4	[30]
θ_{SI}	(rad)	$15.7\times(\pi/180)$ before TDC	[29]
θ_{TDC}	(rad)	0	-
$\Delta\theta$	(rad)	$70\times(\pi/180)$	[33]
M_f	(kg/mol)	0.198	-
M_{N_2}	(kg/mol)	0.028	-
M_{CO_2}	(kg/mol)	0.044	-
M_{H_2O}	(kg/mol)	0.018	-
M_{O_2}	(kg/mol)	0.032	-
$\mathrm{ex}^{ch}_{CO_2}$	(J/mol)	19870	[34]
$\mathrm{ex}^{ch}_{H_2O}$	(J/mol)	900	[34]
$\mathrm{ex}^{ch}_{O_2}$	(J/mol)	3970	[34]
R_{gas}	(J/(mol K))	8.31	-
LHV	(MJ/kg)	42.50	[28]

Table 1: ICE parameters.

4. Internal combustion engine modeling

The exergy model proposed in this manuscript is mean-value, thus, it does not consider the engine's reciprocating behavior (crank-angle) and, instead, it assumes all the phenomena to happen continuously, in a lumped parameter description. In this

section, the mean-value model for the ICE is presented. These results constitute the fundamental preliminary step to build the exergy-based model in Section 5.

The derivation of the ICE model is carried out under the following fundamental assumptions.

Assumption 4.1. The gaseous mixtures are composed by ideal gases only.

Assumption 4.2. The combustion process burns all the available fuel, thus, no unburnt fuel is present in the exhaust gases.

□ Given that a diesel engine works in excess of air ($\lambda > 1$), it is reasonable to assume that all the fuel is burnt.

Assumption 4.3. Each engine operating point is analyzed in steady-state, thus, exhaust transport and torque actuation delays are not modeled.

Assumption 4.4. At a given operating point, the n_{cyl} cylinders of the engine behave in exactly the same manner.

□ This assumption is a direct consequence of the mean-value modeling, where the reciprocating behavior of the whole engine is averaged over time.

4.1. Reference state

In this research activity, the reference state is defined to be at pressure $P_0 = 1\,\text{bar}$ and temperature $T_0 = 298.15\,\text{K}$. In accordance with [21], the atmosphere is assumed to be composed by four species $\sigma \in \mathcal{S} = \{N_2, CO_2, H_2O, O_2\}$ and other components (mostly argon) lumped in one term ($f_{others,0}$). The volume fraction composition of atmospheric air is as follows:

$$f_{N_2,0} = 0.7567,\ f_{CO_2,0} = 0.0003,\ f_{H_2O,0} = 0.0303,\\ f_{O_2,0} = 0.2035,\ f_{others,0} = 0.0092 \tag{1}$$

4.2. Airflow path

The airflow path is modeled considering the mass flow rates at the intake and exhaust manifolds, under the presence of exhaust gas recirculation (EGR). First, the air-fuel equivalence ratio is introduced:

$$\lambda(t) = \frac{\text{AFR}(t)}{\text{AFR}_s}, \quad \text{AFR}(t) = \frac{\dot{m}_a(t)}{\dot{m}_f(t)} \tag{2}$$

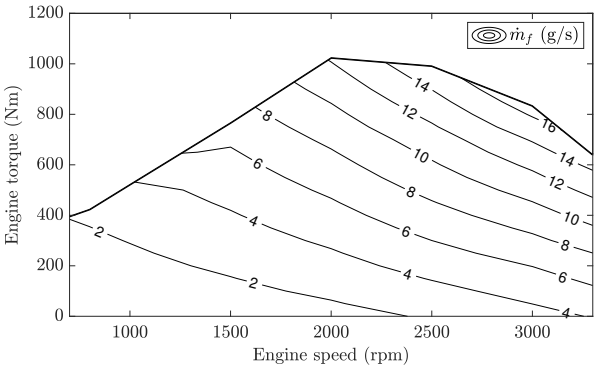

(a) Fuel rate

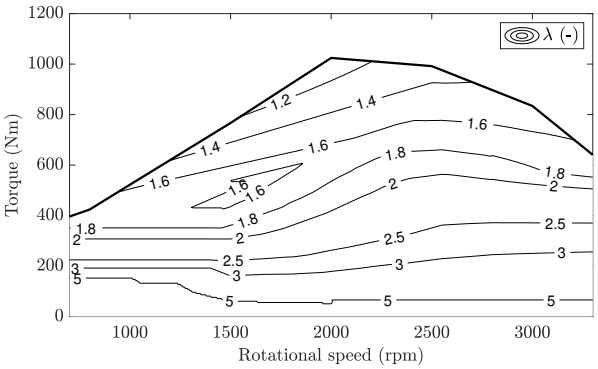

(b) Air-fuel ratio

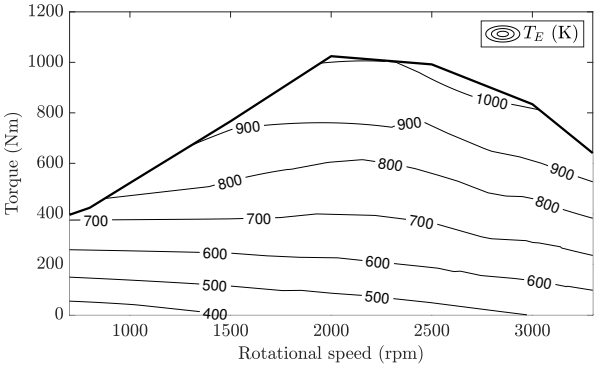

(c) Exhaust gas temperature

Figure 3: Fuel rate ($\dot{m}_f$), air-fuel equivalence ratio (λ), and exhaust gas temperature (T_E) maps.

where AFR_s is the stoichiometric air-fuel ratio, $\dot{m}_a$ and $\dot{m}_f$ are the intake airflow and fuel rates, respectively. The air-fuel equivalence ratio and the fuel rate are functions of the engine operating point:

$$\begin{aligned} \dot{m}_f(t) &= \text{f}_f(\omega_{eng}(t), \text{T}_{eng}(t)) \\ \lambda(t) &= \text{f}_\lambda(\omega_{eng}(t), \text{T}_{eng}(t)) \end{aligned} \tag{3}$$

with T_{eng} and ω_{eng} the engine torque and rotational speed, respectively. In this work, $\dot{m}_f$ and λ come from the maps in Figure 3. Given a diesel engine, the air-fuel equivalence ratio λ is always greater than 1, i.e., the combustion takes place in lean conditions. Relying on Equation (2) to compute $\dot{m}_a$, the intake flow rate is derived as:

$$\dot{m}_I(t) = \dot{m}_a(t) + \dot{m}_{exh}(t) \tag{4}$$

where $\dot{m}_{exh}$ is the portion of exhaust gas introduced by the EGR[1]. According to [28], λ is defined after the perfect mixing between the recirculated gases and fresh air, thus, it already accounts for the presence of recirculated oxygen and nitrogen. Recalling that $\dot{m}_{exh}(t) = x_{EGR}\ \dot{m}_I(t)$ and $\dot{m}_a(t) = (1 - x_{EGR})\dot{m}_I(t)$ [28], Equation (4) is rewritten as follows:

$$\begin{aligned} \dot{m}_I(t) &= \dot{m}_a(t)\left(1 + \frac{x_{EGR}}{1 - x_{EGR}}\right) = \\ &= \dot{m}_a(t)\frac{1}{1 - x_{EGR}} \end{aligned} \tag{5}$$

where x_{EGR} is the EGR rate, i.e., the portion of recirculated gas. Eventually, the exhaust manifold flow rate is obtained as:

$$\dot{m}_E(t) = \dot{m}_I(t) + \dot{m}_f(t) \tag{6}$$

The intake mixture enters the engine at a constant temperature $T_I = 323.15\,\mathrm{K}$ (a reasonable average value for turbocharged diesel engines [35]), instead, the exhaust gas temperature T_E varies according to the engine operating condition (Figure 3c). As a reference for the reader, maps similar to those depicted in Figure 3 can be found in the MathWorks Powertrain Blockset toolbox [36].

4.3. Combustion reaction

According to [37], the combustion reaction in the presence of EGR takes the following form:

$$\begin{aligned} &C_xH_y + \frac{\lambda(t)}{1 - x_{EGR}}\left(x + \frac{y}{4}\right) 3.76N_2 + \frac{x_{EGR}}{1 - x_{EGR}}\left(xCO_2 + \frac{y}{2}H_2O\right) + \\ &+ \left(x + \frac{y}{4}\right)\frac{\lambda(t) - x_{EGR}}{1 - x_{EGR}}O_2 \rightarrow \frac{1}{1 - x_{EGR}}\Big[xCO_2 + \frac{y}{2}H_2O + \\ &+ 3.76\lambda(t)\left(x + \frac{y}{4}\right)N_2 + (\lambda(t) - 1)\left(x + \frac{y}{4}\right)O_2\Big] \end{aligned} \tag{7}$$

[1]The exhaust gas is assumed to be composed by CO_2 and H_2O; NO_x and CO are neglected given their low concentration with respect to the other species [28].

where the coefficients x and y define the fuel (C_xH_y) composition. According to [12], $x = 14.4$ and $y = 24.9$ well describe the average composition of diesel. Given a certain operating condition, the reaction in Equation (7) can be used to compute the mole fraction of the different species composing the intake and exhaust gas, respectively. Thus, the following variables are introduced:

$$\begin{aligned} \det_I(t) &= \frac{\lambda(t)}{1 - x_{EGR}}\left(x + \frac{y}{4}\right) 3.76 + \frac{x_{EGR}}{1 - x_{EGR}}\left(x + \frac{y}{2}\right) + \\ &+ \left(x + \frac{y}{4}\right)\frac{\lambda(t) - x_{EGR}}{1 - x_{EGR}} \\ \det_E(t) &= \frac{1}{1 - x_{EGR}}\Big[x + \frac{y}{2} + 3.76\lambda(t)\left(x + \frac{y}{4}\right) + \\ &+ (\lambda(t) - 1)\left(x + \frac{y}{4}\right)\Big] \end{aligned} \tag{8}$$

with $\det_I$ and $\det_E$ the denominators used to compute the following volume fractions for the reactants (intake gases) and products (exhaust gases):

Intake gases

$$\begin{aligned} f^I_{N_2}(t) &= \frac{\frac{\lambda(t)}{1-x_{EGR}}\left(x + \frac{y}{4}\right) 3.76}{\det_I(t)} = \frac{\nu^I_{N_2}(t)}{\det_I(t)}, \\ f^I_{CO_2}(t) &= \frac{\frac{x_{EGR}}{1-x_{EGR}}x}{\det_I(t)} = \frac{\nu^I_{CO_2}}{\det_I(t)}, \\ f^I_{H_2O}(t) &= \frac{\frac{x_{EGR}}{1-x_{EGR}}\frac{y}{2}}{\det_I(t)} = \frac{\nu^I_{H_2O}}{\det_I(t)}, \\ f^I_{O_2}(t) &= \frac{\frac{\lambda(t)-x_{EGR}}{1-x_{EGR}}\left(x + \frac{y}{4}\right)}{\det_I(t)} = \frac{\nu^I_{O_2}(t)}{\det_I(t)} \end{aligned} \tag{9}$$

Exhaust gases

$$\begin{aligned} f^E_{N_2}(t) &= \frac{\frac{\lambda(t)}{1-x_{EGR}}\left(x + \frac{y}{4}\right) 3.76}{\det_E(t)} = \frac{\nu^E_{N_2}(t)}{\det_E(t)}, \\ f^E_{CO_2}(t) &= \frac{\frac{1}{1-x_{EGR}}x}{\det_E(t)} = \frac{\nu^E_{CO_2}}{\det_E(t)}, \\ f^E_{H_2O}(t) &= \frac{\frac{1}{1-x_{EGR}}\frac{y}{2}}{\det_E(t)} = \frac{\nu^E_{H_2O}}{\det_E(t)}, \\ f^E_{O_2}(t) &= \frac{\frac{\lambda(t)-1}{1-x_{EGR}}\left(x + \frac{y}{4}\right)}{\det_E(t)} = \frac{\nu^E_{O_2}(t)}{\det_E(t)} \end{aligned} \tag{10}$$

Relying on Equations (9) and (10), the molar masses of the gaseous mixtures are computed as follows:

$$M_I(t) = \sum_{\sigma\in\mathcal{S}} f^I_\sigma(t)M_\sigma, \quad M_E(t) = \sum_{\sigma\in\mathcal{S}} f^E_\sigma(t)M_\sigma \tag{11}$$

Starting from Equations (5), (6), (9), and (10), the following molar flow rates are obtained:

$$\dot{n}_I(t) = \frac{\dot{m}_I(t)}{M_I}, \quad \dot{n}_E(t) = \frac{\dot{m}_E(t)}{M_E} \tag{12}$$

4.4. In-cylinder dynamics

To obtain an effective mean-value description of the in-cylinder combustion phenomena, the modeling is first developed in the crank-angle domain and then averaged. To this aim, a single-zone modeling approach, in which the working fluids form *one* thermodynamic system undergoing energy and mass exchange with the surroundings, is employed. In this context, the heat released by combustion is assumed to be evenly distributed throughout the cylinder and no distinction between the burnt/unburnt fraction of the mixture is made. Moreover, spatial homogeneity of pressure and temperature is assumed. According to different authors [31, 30], this is an effective approach to analyze the thermodynamic behavior of ICEs and provides a detailed description of pressure, heat transfer, and temperature.

4.4.1. Crank-angle resolved model

To describe the in-cylinder phenomena, it is fundamental to catch the engine reciprocating behavior. Thus, the crank-angle variable θ is introduced and used to describe the motion of the piston inside the cylinder in terms of distance between the crank shaft and piston (s), swept cylinder volume (V), and combustion chamber surface area (A):

$$\begin{aligned} s(\theta) &= a\ \cos\theta + \sqrt{l^2 - a^2\sin^2\theta} \\ V(\theta) &= V_c + \frac{\pi B^2}{4}(l + a - s(\theta)) = \\ &= \frac{V_{d,tot}/n_{cyl}}{r_c - 1} + \frac{\pi B^2}{4}(l + a - s(\theta)) \\ A(\theta) &= A_{ch} + A_p + \pi B(l + a - s(\theta)) = \\ &= 2\left(\frac{\pi B^2}{4}\right) + \pi B(l + a - s(\theta)) \end{aligned} \tag{13}$$

with a the crank radius, l the rod length, B the cylinder bore, n_{cyl} the number of cylinders, $V_{d,tot}$ the engine displacement, V_c the clearance volume – function of the cylinder displacement $V_{d,tot}/n_{cyl}$ and of the compression ratio r_c –, and A_{ch} and A_p the cylinder head and piston crown surface areas, both equal to $(\pi B^2)/4$.

Starting from Equation (13), the crank-angle derivatives of the swept cylinder volume and combustion chamber surface area are given by:

$$\begin{aligned} \frac{dV}{d\theta} &= \frac{\pi B^2}{4}\left[a\sin\theta\left(\frac{f\cos\theta}{\sqrt{1 - f^2\sin^2\theta}}\right)\right] \\ \frac{dA}{d\theta} &= \pi B\left[a\sin\theta\left(\frac{f\cos\theta}{\sqrt{1 - f^2\sin^2\theta}}\right)\right] \end{aligned} \tag{14}$$

where $f = a/l$. Thus, relying on the first principle of thermodynamics, the following expression for the in-cylinder pressure $\mathcal{P}_{cyl}$ is obtained:

$$\frac{d\mathcal{P}_{cyl}}{d\theta} = \frac{\gamma - 1}{V(\theta)}\left(\frac{d\mathcal{Q}_f}{d\theta} - \frac{d\mathcal{Q}_{cyl}}{d\theta}\right) - \frac{\gamma}{V(\theta)}\mathcal{P}_{cyl}(\theta)\frac{dV}{d\theta} \tag{15}$$

with $\gamma = 1.4 - 0.16/\lambda$ the specific heats ratio (λ is obtained from Equation (3), given an operating point $(\omega_{eng}, \mathrm{T}_{eng})$), $\mathcal{Q}_{cyl}$ the in-cylinder gas to wall heat exchange, and $\mathcal{Q}_f$ the heat released in the combustion process, defined as follows:

$$\frac{d\mathcal{Q}_f}{d\theta} = \frac{dx_{fb}}{d\theta} m_f LHV, \quad m_f = \dot{m}_f \frac{4\pi}{\omega_{eng}} \frac{1}{n_{cyl}} \tag{16}$$

with LHV the fuel lower heating value, m_f the injected fuel per cylinder, and $\dot{m}_f$ the fuel rate computed from Equation (3) at the operating point $(\omega_{eng}, \mathrm{T}_{eng})$, constant over one cycle. The fuel burning rate is computed relying on the Wiebe function [31]:

$$\frac{dx_{fb}}{d\theta} = \frac{c(d+1)}{\Delta\theta}\left(\frac{\theta - \theta_{SC}}{\Delta\theta}\right)^d \exp\left[-c\left(\frac{\theta - \theta_{SC}}{\Delta\theta}\right)^{d+1}\right] \tag{17}$$

where $\Delta\theta$ is the combustion duration, c the combustion efficiency coefficient (controlling if the combustion process leaves unburnt fuel), and d a shaping parameter. The start of combustion angle is defined as $\theta_{SC} = \theta_{SI} - \tau_{id}$, where θ_{SI} is the start of injection angle and τ_{id} the ignition delay [30]:

$$\tau_{id}(\theta) = (0.36 + 0.22 S_p)\exp\left[E_a\left(\frac{1}{R_{gas}\mathcal{T}_{cyl}(\theta_{TDC})} - \frac{1}{17190}\right)\left(\frac{21.2}{\mathcal{P}_{cyl}(\theta_{TDC}) - 12.4}\right)^{0.63}\right] \tag{18}$$

with R_{gas} the ideal gas constant and $E_a = \frac{618840}{CN+25}$ the activation energy, function of the cetane number CN. S_p is the mean piston speed, defined as:

$$S_p = \frac{2L}{60}\frac{60}{2\pi}\omega_{eng} \tag{19}$$

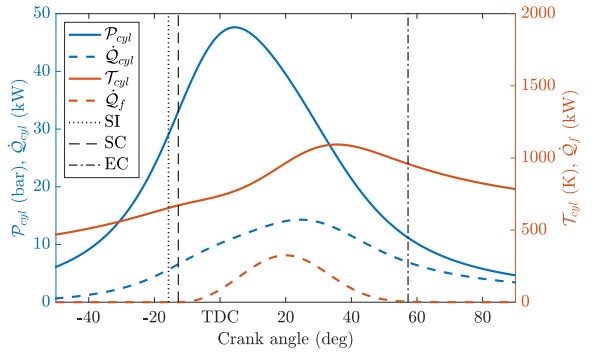

Figure 4: In-cylinder pressure ($\mathcal{P}_{cyl}$), temperature ($\mathcal{T}_{cyl}$), heat transfer ($\dot{\mathcal{Q}}_{cyl}$), and heat released ($\dot{\mathcal{Q}}_f$) profiles are shown for compression and expansion strokes. Simulation results are obtained considering the engine working at 2000 rpm, with 20 mg of injected fuel, λ of 3.7, and 20% EGR.

where L is the stroke. Values for temperatures and pressure at the top dead center θ_{TDC} are estimated assuming a polytropic model for compression: $\mathcal{T}_{cyl}(\theta_{TDC}) = T_I r_c^{\gamma-1}$ and $\mathcal{P}_{cyl}(\theta_{TDC}) = P_I r_c^{\gamma}$ (T_I and P_I are the intake gas temperature and pressure). Therefore, the in-cylinder temperature dynamics is obtained from the ideal gas law (deriving with respect to θ):

$$\mathcal{T}_{cyl}(\theta) = \frac{\mathcal{P}_{cyl}(\theta)V(\theta)}{nR_{gas}},$$
$$\rightarrow \frac{d\mathcal{T}_{cyl}}{d\theta} = \frac{1}{nR_{gas}}\left[\frac{d\mathcal{P}_{cyl}}{d\theta}V(\theta) + \mathcal{P}_{cyl}(\theta)\frac{dV}{d\theta}\right] \tag{20}$$

before injection $n = n_I$ and after injection $n = n_I + m_f/M_f$ (the number of moles is obtained integrating Equation (12) over one cycle).

To compute the thermal exchange between the in-cylinder gas mixture and the walls, the Hohenberg correlation is used and the convective heat transfer coefficient is computed [27]:

$$h_{cyl}(\theta) = 130\ \mathcal{P}_{cyl}(\theta)^{0.8}\mathcal{T}_{cyl}(\theta)^{-0.4}V(\theta)^{-0.06}(S_p + b)^{0.8} \tag{21}$$

where b is a tuning parameter. The convective heat exchange takes the following form:

$$\frac{d\mathcal{Q}_{cyl}}{d\theta} = h_{cyl}(\theta)A(\theta)(\mathcal{T}_{cyl}(\theta) - T_w)\frac{1}{\omega_{eng}} \tag{22}$$

with T_w the average wall temperature.

Simulation outcomes for the engine operating at 2000 rpm, with 20% EGR, are shown in Figure 4.

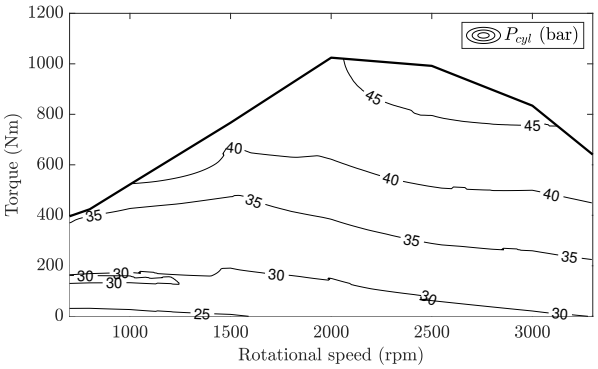

Figure 5: In-cylinder average pressure for each engine operating point. The EGR rate is set to 20%.

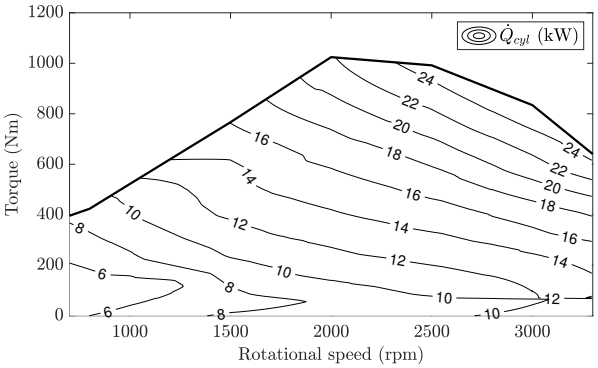

Figure 6: Average heat transfer between the in-cylinder mixture and walls for each engine operating point. The EGR rate is set to 20%.

Results, in terms of $\mathcal{P}_{cyl}$, $\mathcal{T}_{cyl}$, $\dot{\mathcal{Q}}_{cyl}$, and $\dot{\mathcal{Q}}_f$ magnitudes[2], are in line with the literature (see [30], Chapters 10 and 12). Moreover, in accordance with [38], computing the maximum of $\mathcal{P}_{cyl}$ and $\mathcal{T}_{cyl}$ for each engine operating point leads to values confined below 90 bar and 1900 K, respectively. Similarly, the maximum of $\dot{\mathcal{Q}}_{cyl}/A$ assumes values of the order of 2 MW/m^2 (in line with [30] and [39]). Figures for maximum in-cylinder pressure, heat transfer, and temperature are provided in Appendix B. For further details on engine in-cylinder modeling, readers are referred to [30].

4.4.2. Mean-value model

The model described in the previous section is employed to simulate, in the crank-angle domain, the in-cylinder pressure, heat transfer, and temperature profiles for each operating point (ω_{eng}, T$_{eng}$).

[2]To move from the crank-angle to the time domain, the relationship $d\theta = \omega_{eng}dt$ is used, thus, $\dot{\mathcal{Q}} = \frac{d\mathcal{Q}}{d\theta}\omega_{eng}$.

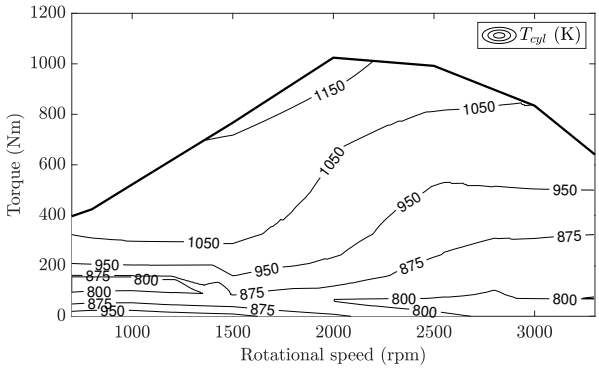

Figure 7: In-cylinder average temperature for each engine operating point. The EGR rate is set to 20%.

These simulation results are used to build static maps providing a mean-value description of the combustion process.

Given the j-th operating point $(\omega_{eng}, \mathrm{T}_{eng})_j$, the following mean values are computed:

$$\bar{\mathcal{V}}_j = \frac{1}{t_2 - t_1} \int_{t_1}^{t_2} \mathcal{V}_j(t) dt \tag{23}$$

where $\mathcal{V}_j = \{\mathcal{P}_{cyl,j}, \dot{\mathcal{Q}}_{cyl,j}, \mathcal{T}_{cyl,j}\}$ and $\bar{\mathcal{V}}_j = \{P_{cyl,j}, \dot{Q}_{cyl,j}, T_{cyl,j}\}$. Equation (23) is evaluated in the time window $(t_2 - t_1)$ – corresponding to 90 deg in the crank-angle domain, i.e., to the engine firing interval[3] –. Therefore, t_1 and t_2 take the following expressions:

- $t_1 = -(\theta_{SI} + \theta_{corr})/\omega_{eng}$;
- $t_2 = (\theta_{EC} + \theta_{corr})/\omega_{eng}$;

with θ_{EC} the crank-angle at the end of combustion. The correction factor $\theta_{corr} = 0.5(\pi/2 - (\tau_{id} + \Delta\theta))$ ensures the window $t_2 - t_1$ to be always corresponding to 90 deg. Computing the mean values over the firing interval allows to accurately capture the average heat released and transferred during the combustion process in a cylinder (in accordance with [39], the highest heat transfer rates take place near the TDC). This is of particular interest for the characterization of the exergy terms related to combustion irreversibilities and heat transfer in Section 5. Recalling Assumption 4.4, and considering one engine cycle of duration t_{cycle}, $\bar{\mathcal{V}}_j$ is an invariant property of the system – i.e., it is a constant describing the combustion process in each of the n_{cyl} cylinders firing one after the other – and can be used to describe the average behavior of the engine at the given operating point $(\omega_{eng}, \mathrm{T}_{eng})_j$.

[3]The firing interval for a V8 engine is computed as $4\pi/n_{cyl} = \pi/2 \rightarrow 90\,\mathrm{deg}$.

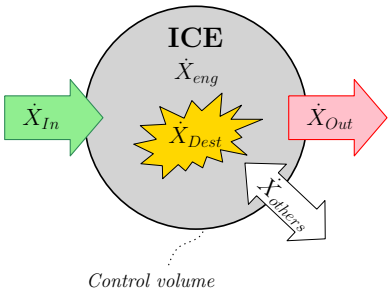

Figure 8: Schematic representation of the exergy transfer and destruction processes in the ICE.

Computing Equation (23) for each operating point $(\omega_{eng}, \mathrm{T}_{eng})_j$ allows to obtain the maps in Figures 5, 6, and 7, useful for the formulation of the exergy balance presented in Section 5. These maps are obtained considering an EGR rate of 20%. As expected from Equations (15), (20), and (22), an increase in the load is related to higher fueling levels and leads to increased in-cylinder pressure, heat transfer, and temperature. Considering Figure 6, the order of magnitude ($\sim$10 kW) is in line with results shown in [28]. From now on, the following notation is used to indicate in-cylinder pressure, heat transfer, and temperature as function of the operating point:

$$\begin{aligned} P_{cyl}(t) &= P_{cyl}(\omega_{eng}(t), \mathrm{T}_{eng}(t)), \\ \dot{Q}_{cyl}(t) &= \dot{Q}_{cyl}(\omega_{eng}(t), \mathrm{T}_{eng}(t)), \\ T_{cyl}(t) &= T_{cyl}(\omega_{eng}(t), \mathrm{T}_{eng}(t)) \end{aligned} \tag{24}$$

5. ICE exergy balance

In this section, the exergy balance for the ICE is formulated according to the open system depicted in Figure 8. The different availability terms are defined with respect to the reference state of Section 4.1. Thus, the overall balance takes the following form:

$$\begin{aligned} \dot{X}_{eng}(t) = & \underbrace{\dot{X}_{fuel,eng}(t) + \dot{X}_{intk,eng}(t)}_{\dot{X}_{In}} + \\ & + \underbrace{\dot{X}_{work,eng}(t) + \dot{X}_{heat,eng}(t) + \dot{X}_{exh,eng}(t)}_{\dot{X}_{Out}} + \\ & + \underbrace{\dot{X}_{comb,eng}(t) + \dot{X}_{fric,eng}(t)}_{\dot{X}_{Dest}} + \dot{X}_{others}(t) \end{aligned} \tag{25}$$

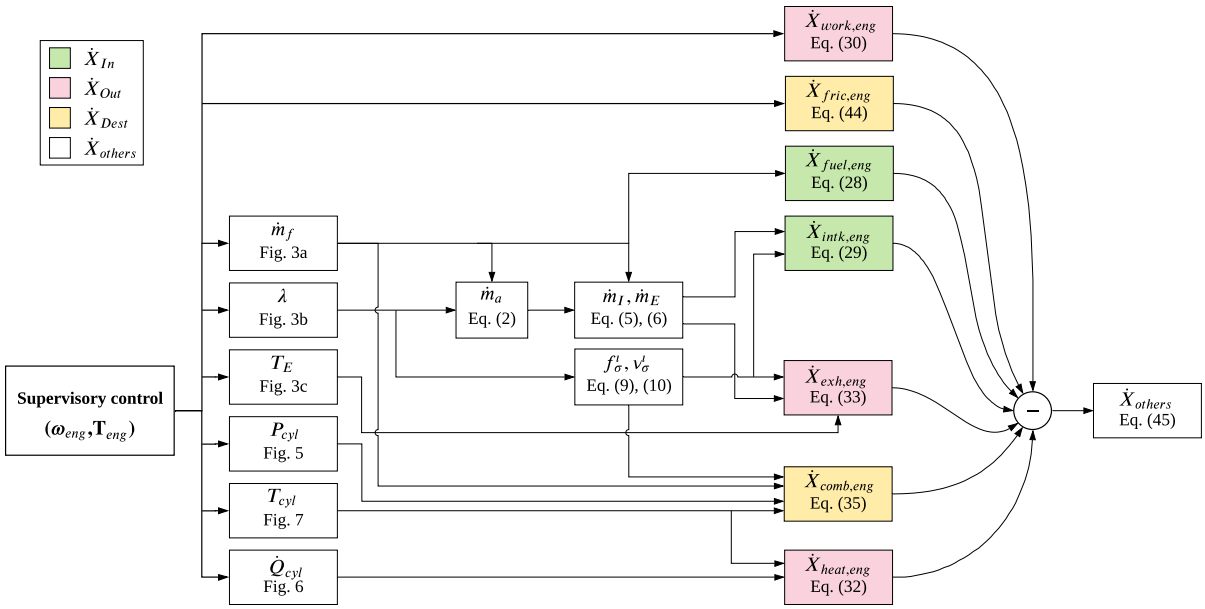

Figure 9: Block diagram of the ICE exergy model.

During the engine operation, fuel and intake air are the positive exergy flows entering the control volume: $\dot{X}_{In} = \dot{X}_{fuel,eng} + \dot{X}_{intk,eng}$. This exergy is transferred out of the control volume ($\dot{X}_{Out}$) because of mechanical work ($\dot{X}_{work,eng}$), heat transfer with the environment ($\dot{X}_{heat,eng}$), and exhaust transport ($\dot{X}_{exh,eng}$). The terms $\dot{X}_{comb,eng}$ and $\dot{X}_{fric,eng}$ indicate the portion of exergy destroyed ($\dot{X}_{Dest}$) by irreversibilities in the combustion process and in the piston motion. The component $\dot{X}_{others}$ accounts for all the unmodeled exergy transfer and destruction phenomena taking place in the engine, e.g., blow-by gases, losses in valves throttling, and nonuniform in-cylinder combustion (not modeled, relying on the single-zone approach).

According to [31] and Assumption 4.3, the engine is assumed to work always at steady-state conditions, thus, transient phenomena between one operating point and the other are neglected. Mathematically, this condition takes the following expression:

$$\int_{cycle} \frac{d\mathcal{X}_{eng}}{d\theta} d\theta = 0 \tag{26}$$

with $\mathcal{X}_{eng}$ the engine exergy state in the crank-angle domain, and "*cycle*" indicating that the integral is computed along one engine cycle, i.e., 720 deg. It can be proven, as shown in Appendix A, that, for the mean-value model, the following condition holds true:

$$\dot{X}_{eng}(t) = 0 \tag{27}$$

The previous result will be employed to compute the term $\dot{X}_{others}$ in Section 5.7.

The overall ICE exergy model, with all the fundamental interactions between blocks, is shown in Figure 9. The sequence of operating points $(\omega_{eng}, \mathrm{T}_{eng})$ are from a supervisory control strategy [40]. The block diagram in Figure 9 has been implemented in MATLAB&SIMULINK.

5.0.1. Fuel

In accordance with [21], the availability associated to the injected fuel is computed as follows:

$$\dot{X}_{fuel,eng}(t) = a_f\ \dot{m}_f(t) = \\ = \left(1.04224 + 0.011925\frac{x}{y} - \frac{0.042}{x}\right) LHV\ \dot{m}_f(t) \tag{28}$$

where a_f is the specific chemical exergy associated with the fuel.

5.1. Intake gas

The intake exergy flow is modeled considering both the chemical and physical exergies entering

the system:

$$\begin{aligned}
&\dot{X}_{intk,eng}(t) = \sum_{\sigma\in\mathcal{S}} \dot{n}_{I,\sigma}(t)(\psi^I_{ch,\sigma}(t) + \psi^I_{ph,\sigma}(t)),\\
&\dot{n}_{I,\sigma}(t) = \dot{n}_I(t) f^I_\sigma(t),\\
&\psi^I_{ph,\sigma}(t) = (h_\sigma(T_I) - T_0 s_\sigma(T_I)) - (h^\star_\sigma(T_0) - T_0 s^\star_\sigma(T_0))\,,\\
&\psi^I_{ch,\sigma}(t) = R_{gas} T_0 \log\left(\frac{f^\star_\sigma(t)}{f_{\sigma,0}}\right) = R_{gas} T_0 \log\left(\frac{f^I_\sigma(t)}{f_{\sigma,0}}\right)
\end{aligned} \tag{29}$$

with $\psi^I_{ph,\sigma}$ the physical exergy, modeling the work potential between the current system state (at T_I and P_I) and the restricted state, and $\psi^I_{ch,\sigma}$ the chemical exergy, accounting for the different chemical composition between the restricted (i.e., the intake manifold composition) and reference state. The term $\dot{n}_{I,\sigma}$ indicates the fraction of the total intake molar flow rate for a particular species σ. General concepts on the modeling of exergy fluxes can be found in [41].

5.2. Mechanical work

A portion of the availability introduced in the engine, modeled as in Equations (28) and (29), is converted into useful mechanical work (brake work):

$$\dot{X}_{work,eng}(t) = -\mathrm{T}_{eng}(t)\omega_{eng}(t) = -P_{eng}(t) \tag{30}$$

The percentage of the fuel availability converted into mechanical work is the engine efficiency according to the second law of thermodynamics, i.e.,

$$\varepsilon(t) = \frac{X_{work,eng}(t)}{X_{fuel,eng}(t)} \tag{31}$$

where $X_{work,eng}$ and $X_{fuel,eng}$ are obtained integrating over time the corresponding exergy rate terms.

5.3. Heat exchange

The exergy transfer, due to heat exchange between the in-cylinder mixture and the cylinder's walls, is computed relying on Figures 6 and 7:

$$\dot{X}_{heat,eng}(t) = \left(1 - \frac{T_0}{T_{cyl}(t)}\right)\left(-\dot{Q}_{cyl}(t)\right) \tag{32}$$

where the term inside brackets is the Carnot heat engine efficiency. The temperature T_{cyl}, at which the thermal exchange occurs, must be higher than the reference state temperature T_0. Also, as the temperature T_{cyl} decreases, the exergy transfer is reduced because the Carnot efficiency, function of the ratio between the low- and high-temperature reservoirs, is reduced. The minus before $\dot{Q}_{cyl}$ is modeling the direction of the heat transfer: from inside the engine to the environment.

5.4. Exhaust gas

The exhaust gas exergy transfer is modeled in accordance with Section 5.1, i.e., considering the chemical and physical exergy fluxes for each species σ:

$$\begin{aligned}
&\dot{X}_{exh,eng}(t) = -\sum_{\sigma\in\mathcal{S}} \dot{n}_{E,\sigma}(t)(\psi^E_{ch,\sigma}(t) + \psi^E_{ph,\sigma}(t)),\\
&\dot{n}_{E,\sigma}(t) = \dot{n}_E(t) f^E_\sigma(t),\\
&\psi^E_{ph,\sigma}(t) = (h_\sigma(T_E(t)) - T_0 s_\sigma(T_E(t))) - (h^\star_\sigma(T_0) - T_0 s^\star_\sigma(T_0))\,,\\
&\psi^E_{ch,\sigma}(t) = R_{gas} T_0 \log\left(\frac{f^\star_\sigma(t)}{f_{\sigma,0}}\right) = R_{gas} T_0 \log\left(\frac{f^E_\sigma(t)}{f_{\sigma,0}}\right)
\end{aligned} \tag{33}$$

with the term $\dot{n}_{E,\sigma}$ indicating the fraction of the total exhaust molar flow rate for a species σ and T_E being the exhaust temperature for a given operating condition (as shown in Figure 3c). In this context, exergy is transferred outside the engine, leading to an availability decrease.

5.5. Combustion irreversibilities

Combustion irreversibilities are function of the reaction rate and of the variations of the chemical potential between reactants and products. Thus, the entropy generation in chemical reactions ($\dot{S}_{gen,eng}$), formulated as in [42], is employed to model the exergy destruction due to combustion irreversibilities:

$$\begin{aligned}
\dot{X}_{comb,eng}(t) &= -T_0 \dot{S}_{gen,eng}(t) =\\
&= \frac{T_0}{T_{cyl}(t)} \Bigg\{ \underbrace{-\nu_f \mu_f + \sum_{\sigma\in\mathcal{S}} \left[-\nu^I_\sigma(t)\mu^I_\sigma(t)\right]}_{Reactants} + \underbrace{\nu^E_\sigma(t)\mu^E_\sigma(t)}_{Products} \Bigg\} \dot{\xi}(t)
\end{aligned} \tag{36}$$

with I and E indicating the gaseous species entering, the reactants, and exiting the system, the products, and ν the stoichiometric coefficients of the combustion reaction in Equation (7). The chemical reaction is assumed to take place at the average in-cylinder temperature T_{cyl} (Figure 7). Thus, for each gaseous species σ in $\iota \in \{I, E\}$, the chemical potential μ is defined as:

$$\mu^\iota_\sigma(t) = g_\sigma(t) + R_{gas} T_{cyl}(t) \log\left(\frac{f^\iota_\sigma(t) P_{cyl}(t)}{P_0}\right) \tag{37}$$

with $g_\sigma(t) = h_\sigma(T_{cyl}(t)) - T_{cyl}(t) s_\sigma(T_{cyl}(t))$ the Gibbs free energy. It is worth to mention that, the entropy generation $\dot{S}_{gen,eng}$, is function of T_{cyl}: the higher the temperature, the higher the combustion efficiency and the lower the entropy generation. For reactants, the minus in Equation (36) indicates that

$$a_f = \left(1.04224 + 0.011925\frac{x}{y} - \frac{0.042}{x}\right) LHV = \overbrace{\left[g_f + \left(x + \frac{y}{4}\right) g_{O_2} - x g_{CO_2} - \frac{y}{2} g_{H_2O}\right]_{(T_0,P_0)}}^{\boldsymbol{\alpha}} + x\ \mathrm{ex}^{ch}_{CO_2} + \frac{y}{2}\mathrm{ex}^{ch}_{H_2O} - \left(x + \frac{y}{4}\right)\mathrm{ex}^{ch}_{O_2} \tag{34}$$

$$\begin{aligned}
\dot{X}_{comb,eng}(t) &= \frac{T_0}{T_{cyl}(t)}\Big\{ - \nu_f \mu_f + \sum_{\sigma\in\mathcal{S}} \left[- \nu^I_\sigma(t)\mu^I_\sigma(t) + \nu^E_\sigma(t)\mu^E_\sigma(t)\right]\Big\}\dot{n}_f(t) = \\
&= -\frac{T_0}{T_{cyl}(t)}\Bigg[g_f + g_{N_2}(t)\left(\nu^I_{N_2}(t) - \nu^E_{N_2}(t)\right) + g_{CO_2}(t)\left(\nu^I_{CO_2} - \nu^E_{CO_2}\right) + g_{H_2O}(t)\left(\nu^I_{H_2O} - \nu^E_{H_2O}\right) + g_{O_2}(t)\left(\nu^I_{O_2}(t) - \nu^E_{O_2}(t)\right) + \\
&\quad + \nu^I_{N_2}(t) R_{gas} T_{cyl}(t) \log\left(\frac{f^I_{N_2}(t) P_{cyl}(t)}{P_0}\right) + \nu^I_{CO_2} R_{gas} T_{cyl}(t) \log\left(\frac{f^I_{CO_2}(t) P_{cyl}(t)}{P_0}\right) + \\
&\quad + \nu^I_{H_2O} R_{gas} T_{cyl}(t) \log\left(\frac{f^I_{H_2O}(t) P_{cyl}(t)}{P_0}\right) + \nu^I_{O_2}(t) R_{gas} T_{cyl}(t) \log\left(\frac{f^I_{O_2}(t) P_{cyl}(t)}{P_0}\right) - \\
&\quad - \nu^E_{N_2}(t) R_{gas} T_{cyl}(t) \log\left(\frac{f^E_{N_2}(t) P_{cyl}(t)}{P_0}\right) - \nu^E_{CO_2} R_{gas} T_{cyl}(t) \log\left(\frac{f^E_{CO_2}(t) P_{cyl}(t)}{P_0}\right) - \\
&\quad - \nu^E_{H_2O} R_{gas} T_{cyl}(t) \log\left(\frac{f^E_{H_2O}(t) P_{cyl}(t)}{P_0}\right) - \nu^E_{O_2}(t) R_{gas} T_{cyl}(t) \log\left(\frac{f^E_{O_2}(t) P_{cyl}(t)}{P_0}\right)\Bigg]\dot{n}_f(t) = \\
&= -\frac{T_0}{T_{cyl}(t)}\Bigg\{ g_f - x g_{CO_2}(t) - \frac{y}{2} g_{H_2O}(t) + \left(x + \frac{y}{4}\right) g_{O_2}(t) + \frac{\lambda(t)}{1 - x_{EGR}}\left(x + \frac{y}{4}\right) 3.76 R_{gas} T_{cyl}(t) \log\left(\frac{f^I_{N_2}(t)}{f^E_{N_2}(t)}\right) + \\
&\quad + R_{gas} T_{cyl}(t) \sum_{\sigma\in\mathcal{S}\setminus\{N_2\}} \left[\nu^I_\sigma(t) \log\left(\frac{f^I_\sigma(t) P_{cyl}(t)}{P_0}\right) - \nu^E_\sigma(t) \log\left(\frac{f^E_\sigma(t) P_{cyl}(t)}{P_0}\right)\right]\Bigg\}\dot{n}_f(t)
\end{aligned} \tag{35}$$

species are consumed and converted into products (for which a "plus" sign is used). The extent of reaction ξ models the reactants to products conversion rate:

$$\dot{\xi}(t) = \frac{1}{\nu_f}\dot{n}_{C_xH_y}(t) = \frac{1}{\nu^I_\sigma(t)}\dot{n}_{I,\sigma}(t) = \frac{1}{\nu^E_\sigma(t)}\dot{n}_{E,\sigma}(t) \tag{38}$$

with $\dot{n}_{C_xH_y}$ the reacted fuel. Assuming the fuel injected $\dot{n}_f$, for a given operating point, to completely react with the intake gas (see Assumption 4.2), and recalling that $\nu_f = 1$, the following equality holds:

$$\dot{\xi}(t) = \dot{n}_{C_xH_y}(t) = \dot{n}_f(t) \tag{39}$$

which leads to:

$$\dot{n}_{I,\sigma}(t) = \nu^I_\sigma \dot{n}_f(t), \;\; \dot{n}_{E,\sigma}(t) = \nu^E_\sigma \dot{n}_f(t) \tag{40}$$

To compute the hydrocarbons chemical potential $\mu_f = g_f$ (the fuel is considered in its liquid state), the expression of the specific fuel exergy a_f is recalled. In accordance with [34, 43], considering a simplified combustion reaction scheme:

$$C_xH_x + \left(x + \frac{y}{4}\right) O_2 \rightarrow x CO_2 + \frac{y}{2} H_2O \tag{41}$$

and assuming the fuel to enter the system at P_0 and T_0, the work that can be obtained through the reaction of C_xH_y is shown in Equation (34). Therefore, inverting Equation (34), the fuel Gibbs free energy is obtained:

$$g_f = \left(1.04224 + 0.011925\frac{x}{y} - \frac{0.042}{x}\right) LHV - \boldsymbol{\alpha} \tag{42}$$

According to [12], modifications in the fuel temperature lead to negligible variations in the fuel availability a_f, thus, Equation (42) can be considered a good estimate of the fuel Gibbs free energy at T_{cyl} and P_{cyl}.

Starting from Equation (36), while relying on Equations (37), (39), (40), and (42), the final expression for $\dot{X}_{comb,eng}$ is given in Equation (35).

5.6. Frictions

According to [30], the engine frictions, in terms of components motion and turbulent dissipation, are modeled according to the friction mean effective pressure (FMEP):

$$\mathrm{FMEP}(t) = 1000\left[C_1 + C_2\omega_{eng}(t) + C_3 S_p(t)^2\right] \tag{43}$$

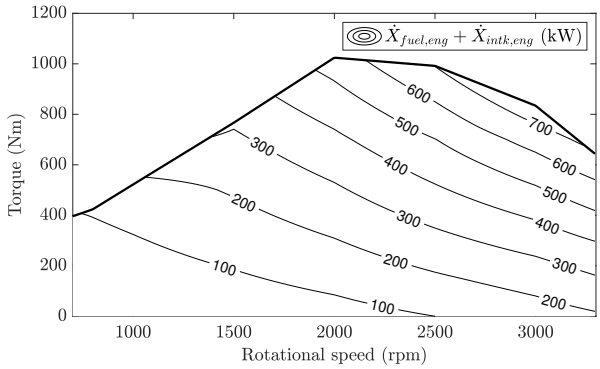

Figure 10: Availability introduced in the engine: $\dot{X}_{fuel,eng} + \dot{X}_{intk,eng}$.

where C_1, C_2, and C_3 are identified coefficients. Eventually, the corresponding exergy destruction term is computed as follows:

$$\begin{aligned}\dot{X}_{fric,eng}(t) &= -\frac{1}{t_{cycle}(t)}\text{FMEP}(t)\ V_{d,tot} = \\ &= -\frac{\omega_{eng}(t)}{4\pi}\text{FMEP}(t)\ V_{d,tot}\end{aligned} \tag{44}$$

with $t_{cycle}(t) = 4\pi/\omega_{eng}(t)$ the engine cycle time for a given operating point and considering a four stroke engine.

5.7. Others

Recalling Equation (27), the exergy term for the in-cylinder exergy transfer and destruction unmodeled phenomena is computed as follows:

$$\begin{aligned}\dot{X}_{others}(t) = -\big[&\dot{X}_{fuel,eng}(t) + \dot{X}_{intk,eng}(t) + \\ &+ \dot{X}_{work,eng}(t) + \dot{X}_{heat,eng}(t) + \dot{X}_{exh,eng}(t) + \\ &+ \dot{X}_{comb,eng}(t) + \dot{X}_{fric,eng}(t)\big]\end{aligned} \tag{45}$$

6. Results

6.1. Exergy maps

In this section, a steady-state exergy analysis is carried out for each engine operating point. All simulation results are obtained considering the parameters listed in Table 1.

The availability $\dot{X}_{In}$ introduced in the engine, and given by the summation of the injected fuel and the intake air exergies, is shown in Figure 10. The intake air enters the cylinder at a temperature T_I, close to the reference state temperature T_0. Thus, in accordance with [17], the associated exergy contribution is almost negligible and accounts for at most 1% of the total input exergy. The remaining 99% comes from the fuel availability defined in Equation (28). According to Section 5 and recalling Figure 8, a portion of $\dot{X}_{In}$ is transferred outside the system by mechanical work, heat exchange with the cylinder's walls, and exhaust gas flow ($\dot{X}_{Out}$). The remaining input availability is destroyed in two principal ways ($\dot{X}_{Dest}$): frictions and combustion irreversibilities. To assess the relative contribution of each exergy transfer and destruction term, the following relationship is introduced:

$$\dot{X}_k\ (\%) = \frac{\dot{X}_k}{\dot{X}_{fuel,eng} + \dot{X}_{intk,eng}} \times 100 \tag{46}$$

with $\dot{X}_k \in \mathcal{K} = \{\dot{X}_{fuel,eng}, \dot{X}_{intk,eng}, \dot{X}_{work,eng}, \dot{X}_{heat,eng}, \dot{X}_{exh,eng}, \dot{X}_{comb,eng}, \dot{X}_{fric,eng}, \dot{X}_{others}\}$.

Increasing the load leads to higher in-cylinder pressure, heat transfer, and temperature (Figures 5, 6, and 7). In this scenario, the percentage contribution related to combustion reactions decreases: from 40% at low loads to around 30% (Figure 11d). This is reasonable since, at higher in-cylinder temperatures, the combustion becomes more efficient and entropy generation is reduced. Conversely, the efficiency ε – defined in Equation (31) – increases, leading to higher availability transfer due to mechanical work generation (up to 38%), as shown in Figure 11a. An increased load means also increased exhaust gas temperatures (T_E), leading to higher availability transfer due to exhaust gases (Figure 11c).

Recalling Equation (32), an increasing load increases the exergy transfer due to heat exchange (the Carnot efficiency increases). However, compared to the other exergy transfer and destruction terms, the relative contribution becomes smaller. This effect is emphasized at high engine rotational speeds because of the lower available time for heat exchanges. As shown in Figure 11b, the contribution related to heat transfer goes from 12%, at low loads and speed, to 2.5%, at high loads and speed.

According to Section 5.6, the exergy term related to frictions is a function of the engine rotational speed only and increases with it. At a given speed, increasing the load leads to no variation of the friction exergy term, thus, its relative contribution decreases, reaching 5% (Figure 11e). At low loads, a contribution of 25% is obtained: this is in line with the fact that the efficiency ε is reduced.

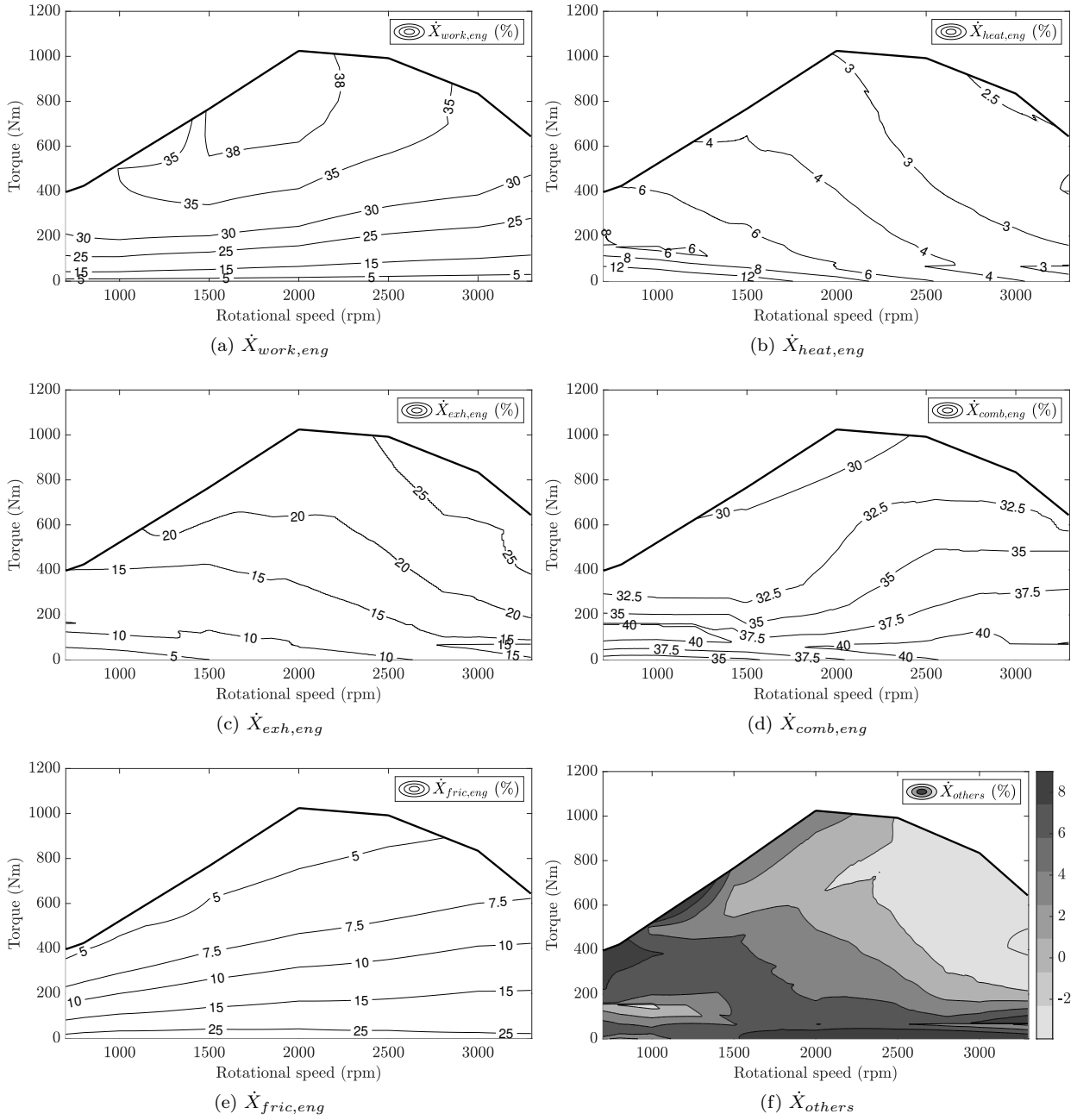

(a) $\dot{X}_{work,eng}$ (b) $\dot{X}_{heat,eng}$

(c) $\dot{X}_{exh,eng}$ (d) $\dot{X}_{comb,eng}$

(e) $\dot{X}_{fric,eng}$ (f) $\dot{X}_{others}$

Figure 11: Percentage contribution of the different exergy transfer and destruction terms with respect to $\dot{X}_{fuel,eng} + \dot{X}_{intk,eng}$. Considering $\dot{X}_{others}$, colors are used to improve readability.

The term $\dot{X}_{others}$ accounts for all the unmodeled exergy transfer and destruction phenomena. In accordance with results shown in [21, 12], this term accounts for 8 to 2% (Figure 11f). On average, a contribution of 3.5% is obtained.

In Table 2, simulation data for the engine operating at 1400 rpm and 258 Nm are compared to results from [16] obtained for a turbocharged diesel engine with a cylinder displacement of 1 liter (similar to the ICE considered in this work, for which the cylinder displacement is 0.8 liters). Given the different engines, and the dissimilar underlying control

Exergy term (%)	*Ref. [16]*	*Engine maps (Figure 11)*
$\dot{X}_{work,eng}$	34.4	32.5
$\dot{X}_{heat,eng}$	5.7	6.0
$\dot{X}_{exh,eng}$	13.6	12.2
$\dot{X}_{comb,eng}+\dot{X}_{fric,eng}+$ $+\dot{X}_{others}$	46.3	49.3

Table 2: Comparison of exergy terms and irreversibilities at 1400 rpm and 258 Nm. In [16], terms $\dot{X}_{comb,eng}$, $\dot{X}_{fric,eng}$, and $\dot{X}_{others}$ are lumped together.

strategies, the comparison is not rigorous. However, it provides useful insights showing that the outcomes of the proposed modeling strategy are in line with the results in the literature. As a final remark, it is worth mentioning that values in Figure 11 are comparable to the ranges reported in [12] for diesel engines, i.e., the indicated work rate ($\dot{X}_{work,eng} + \dot{X}_{fric,eng}$) accounts for 40-45%, the heat transfer term for ∼10%, the exhaust gas for 10-20%, and the combustion irreversibilities for ∼25% (at full load).

6.2. Exergy analysis over a driving cycle

The exergy analysis is performed considering the DCE5 Urban Assault military driving cycle, shown in Figure 12. The whole model of the series HEV in Figure 1, described in [25], is simulated. An energy management strategy based on the Pontryagin Minimum Principle (PMP) [26], optimizes the power split between the battery pack and the ICE, minimizing a cost function accounting for fuel consumption while ensuring charge sustaining conditions. The optimal sequence of engine operating points (i.e., the *Supervisory control* of the block diagram in Figure 9), for an EGR rate of 20%, is shown in Figure 13. It is worth to mention that each operating point is analyzed under Assumption 4.3. Focusing on the ICE only, the analyses of other components of the powertrain and of the optimal power split are out of the scope of this work.

Figure 14 shows the exergy balance simulation results considering four different EGR rates, namely: 0, 10, 20, and 30% (a reasonable range for diesel engines [31]). In this scenario, the contribution of each exergy term is computed as:

$$X_k\ (\%) = \frac{X_k}{X_{fuel,eng} + X_{intk,eng}} \times 100 \qquad (47)$$

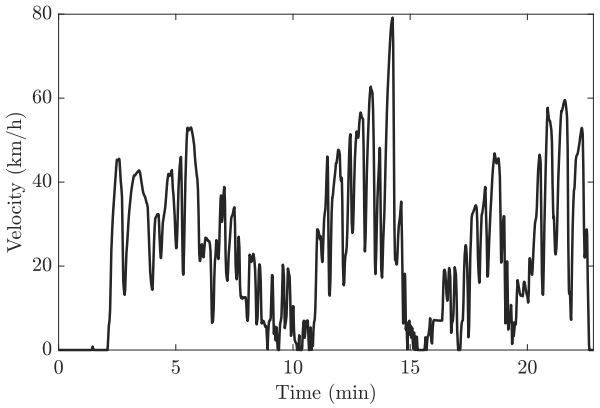

Figure 12: DCE5 Urban Assault driving cycle.

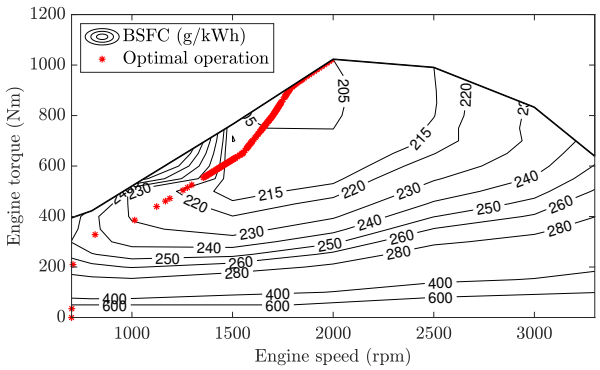

Figure 13: Optimal sequence of engine operating points considering an EGR rate of 20%.

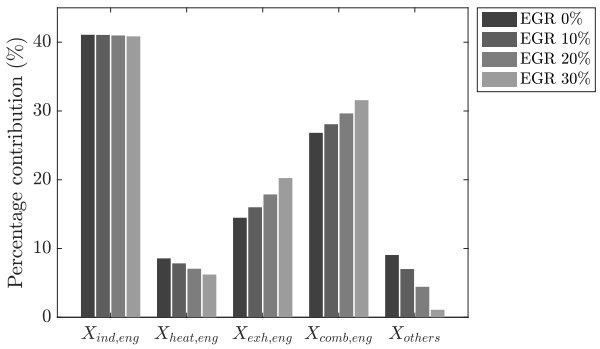

Figure 14: Comparison of exergy terms and irreversibilities for different EGR rates.

with X_k obtained integrating the corresponding exergy rate term inside the set $\mathcal{K}$, introduced for Equation (46). In this context, the summation of the mechanical work and friction terms ($X_{work,eng} + X_{fric,eng}$) is the indicated work $X_{ind,eng}$.

Given an engine operating point and equivalence

ratio λ, an increment of the EGR rate leads to additional recirculated exhaust gas mass and to an increase of the in-cylinder thermal inertia. This causes a decrease of the in-cylinder temperature T_{cyl}, of the heat transfer $\dot{Q}_{cyl}$, and, consequently, of the exergy term $X_{heat,eng}$. At lower temperatures, the combustion reaction becomes less efficient, leading to an increased entropy generation and to a higher contribution of $X_{comb,eng}$ to the total exergy balance. The additional mass of exhaust gas introduced in the cylinder must be transferred outside the system, increasing $X_{exh,eng}$. The percentage contribution of the indicated work to the overall balance is, in practice, not changing varying the EGR, with the efficiency ε being 33%. Only a slight reduction, lower than 0.5%, is caused by the intake flux exergy increase ($X_{intk,eng}$). The term X_{others} remains constrained to values in line with the literature and reaches a maximum for 0% EGR; this latter condition is, however, unlikely for diesel engines, because it would lead to unacceptable NO_x emissions.

The EGR rate x_{EGR}, is generally a function of time and could be an additional map to be used together with the information provided in Figure 3. In this work, given that an EGR map was not available, the authors chose to use a constant EGR rate (x_{EGR}) and perform the sensitivity analysis above.

7. Conclusions

In this work, the derivation of a comprehensive mean-value exergy-based model for compression ignition diesel ICEs is shown. Starting from the mean-value modeling of the in-cylinder behavior, the exergy balance is solved for each engine operating point and static maps, describing the availability transfer and destruction as function of the engine speed and load, are obtained. For the first time, the concept of availability is extended to model the whole engine operating field and not, as it has been done so far, a restricted set of operating points. This allows to extract useful information on the engine efficiency (and inefficiency) and quantify how a modification of the operating conditions affects the exergy balance.

The method proposed in this paper has the potential of being disruptive in the vehicular community. As a matter of fact, the outcomes of the approach are (low computational burden) static maps providing a mean-value and control-oriented description of the engine, that could enable the development of optimized "exergy management strategies" aiming at minimizing the overall operational losses. Other than some engine technical specifications, the only information needed to compute the balance is the BSFC, λ, exhaust gas temperature, and EGR rate maps (typically all available to engine practitioners). If crank-angle resolved in-cylinder pressure, heat transfer, and temperature data are accessible for all the operating points, these should be used for the direct computation of maps in Figures 5, 6, and 7, without the need of implementing and calibrating the in-cylinder model described in Section 4.4.1. It is worth mentioning that, for a given engine, the static maps must be computed only once.

Ultimately, the proposed approach can be applied to any vehicle or device equipped with an ICE (and not only to series HEVs) and easily extended to spark ignition engines (the principal difference is that fuel is injected into the cylinder during the intake stroke).

Acknowledgments

Unclassified. DISTRIBUTION STATEMENT A. Approved for public release; distribution is unlimited. Reference herein to any specific commercial company, product, process, or service by trade name, trademark, manufacturer, or otherwise does not necessarily constitute or imply its endorsement, recommendation, or favoring by the United States Government or the Dept. of the Army (DoA). The opinions of the authors expressed herein do not necessarily state or reflect those of the United States Government or the DoD, and shall not be used for advertising or product endorsement purposes.

Appendix A.

Proposition A.1. In steady-state conditions, the mean-value availability introduced in the engine at a point in time t, denoted by $\dot{X}_{In}$, is transferred via mass, heat, and work outside the system ($\dot{X}_{Out}$) or irreversibly destroyed ($\dot{X}_{Dest}$). The summation of these terms satisfies the following equality:

$$\dot{X}_{eng}(t) = \dot{X}_{In}(t) + \dot{X}_{Out}(t) + \dot{X}_{Dest}(t) = 0 \quad \text{(A.1)}$$

Remark A.1. Given the model developed in Section 4 and considering one engine operating point, $\dot{X}_{In}$,

$\dot{X}_{Out}$, and $\dot{X}_{Dest}$ are constant. Therefore, $\dot{X}_{eng}$ is also a constant value.

Remark A. 2. Proposition A.1 is formulated under the assumption that $\dot{X}_{others} = 0$. The proof proposed in this appendix can be extended to the scenario $\dot{X}_{others} \neq 0$ adding to the equality in Equation (A.1) the term $\dot{X}_{others}$ (similarly to Equation (25)).

Proof. First, the proof is carried out considering one cylinder, then, results are extended to a n_{cyl} cylinders engine. According to [31], and considering one cylinder cycle, at steady-state (i.e., at a given operating point) the following condition holds:

$$\int_{cycle} \frac{d\mathcal{X}_{eng}}{d\theta} d\theta = 0 \tag{A.2}$$

For convenience, recalling that $d\theta = \omega_{eng} dt$, Equation (A.2) is rewritten in the time domain as:

$$\int_0^{t_{cycle}} \dot{\mathcal{X}}_{eng}(t) dt = 0 \tag{A.3}$$

The mean-value model assumes that combustion takes place continuously over one cycle. Therefore, we can write the following integral:

$$\int_0^{t_{cycle}} \dot{X}_{eng}(t) dt = \delta \tag{A.4}$$

with $\delta \in \mathbb{R}$. Given Remark A.1, $\dot{X}_{eng}$ is a constant value and Equation (A.4) is rewritten as:

$$\dot{X}_{eng} \int_0^{t_{cycle}} 1 \; dt = \delta \rightarrow \dot{X}_{eng} = \frac{\delta}{t_{cycle}} \tag{A.5}$$

From Equation (A.3), we know that the exergy balance over one cycle is zero, consequently:

$$\dot{X}_{eng} = \frac{\delta}{t_{cycle}} = 0 \tag{A.6}$$

Considering n_{cyl} cylinders working at steady-state conditions, and recalling Assumption 4.4, Equation (A.6) can be easily extended as follows:

$$\dot{X}_{eng} = n_{cyl} \times \frac{\delta}{t_{cycle}} = 0 \tag{A.7}$$

□

The proof is developed for one engine cycle. Considering N cycles, the following result holds: $\dot{X}_{eng} = N \times (n_{cyl}\delta / t_{cycle}) = 0$.

Appendix B.

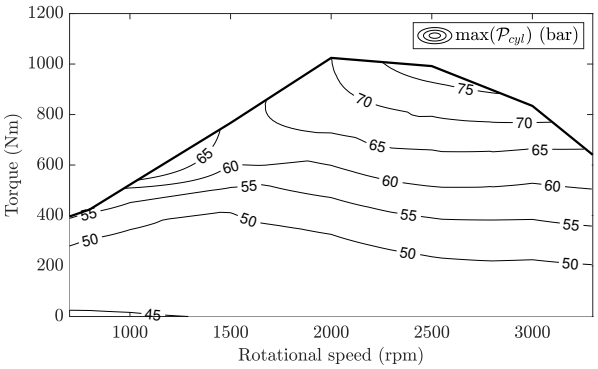

Figure B.15: Maximum of $\mathcal{P}_{cyl}$ for each engine operating point. Results obtained considering the parameters listed in Table 1.

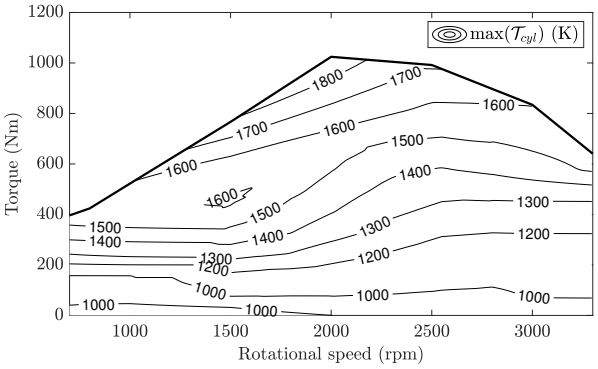

Figure B.16: Maximum of $\mathcal{T}_{cyl}$ for each engine operating point. Results obtained considering the parameters listed in Table 1.

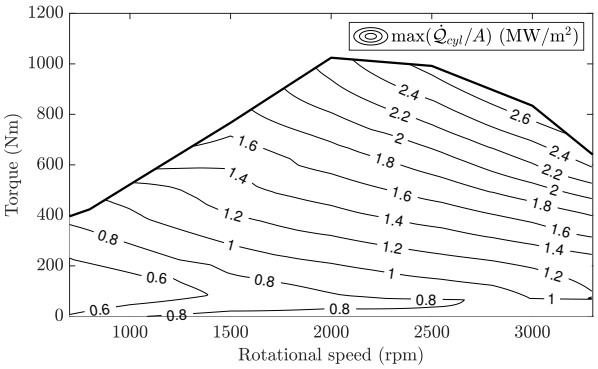

Figure B.17: Maximum of $\dot{\mathcal{Q}}_{cyl}/A$ for each engine operating point. Results obtained considering the parameters listed in Table 1.

Notation

0	Reference state
$\star$	Restricted state
σ	Chemical species
ι	Index indicating intake and exhaust: $\iota \in \{I, E\}$
j	Engine operating point
k	Index to indicate an exergy term in a set $\mathcal{K}$
$\mathcal{K}$	Set collecting exergy terms
$\mathcal{S}$	Set collecting the chemical species σ, defined as $\{N_2, CO_2, H_2O, O_2\}$
$d\chi/d\theta$	Crank-angle derivative of a variable χ
$\dot{\chi}$	Time derivative of a variable χ
a, f, s	Subscripts for air, fuel, and stoichiometric, respectively
exh	Exhaust gas introduced in the engine by the EGR
I, E	Intake and exhaust
EGR	Exhaust gas recirculation
EC	End of combustion
SC	Start of combustion
SI	Start of injection
TDC	Top dead center

Nomenclature

ε	Second law efficiency $(-)$
γ	Specific heats ratio $(-)$
λ	Air-fuel equivalence ratio $(-)$
b	Hohenberg model coefficient $(-)$
c, d	Wiebe function coefficients $(-)$
CN	Cetane number $(-)$
f	Mole fraction $(-)$
N	Number of cycles $(-)$
n_{cyl}	Number of cylinders $(-)$
r_c	Compression ratio $(-)$
x, y	Fuel chemical formula coefficients $(-)$
x_{EGR}	EGR rate $(-)$
x_{fb}	Fuel burning rate (Wiebe function) $(-)$
t, dt	Time and its differential (s)
t_{cycle}	Engine cycle time (s)
ξ	Extent of reaction (1/s)
a	Crank radius (m)
l	Rod length (m)
B	Bore (m)
L	Stroke (m)
A	Combustion chamber area (m^2)
A_p	Cylinder head surface area (m^2)
A_{ch}	Piston crown surface area (m^2)
V	Combustion chamber volume (m^3)
$V_{d,tot}$	Engine displacement (m^3)
S_p	Mean piston speed (m/s)
AFR	Air-fuel ratio (mol)
ν	Stoichiometric coefficient (mol)
det	Summation of stoichiometric coefficients (mol)
$n, \dot{n}$	Moles and molar flow rate (mol), (mol/s)
$m, \dot{m}$	Mass and mass flow rate (kg), (kg/s)
M	Molar mass (kg/mol)
$FMEP$	Friction mean effective pressure (Pa)
C_1, C_2, C_3	FMEP coefficients (kPa),(s kPa),(s^2kPa/m^2)
P_0	Reference state pressure (bar)
P_I	Intake gas pressure (bar)
P_{cyl}	In-cylinder gas temperature (bar)
$\mathcal{P}_{cyl}$	In-cylinder pressure, crank-angle domain (bar)
T_0	Reference state temperature (K)
T_I, T_E	Intake and exhaust gas temperature (K)
T_w	Average wall temperature (K)
T_{cyl}	In-cylinder gas temperature (K)
$\mathcal{T}_{cyl}$	In-cylinder gas temperature, crank-angle domain (K)
Q_{cyl}	In-cylinder gas to wall thermal exchange (J)
$\mathcal{Q}_{cyl}$	In-cylinder gas to wall thermal exchange, crank-angle domain (J)
$\mathcal{Q}_f$	Heat release during combustion (J)
μ	Chemical potential (J/mol)
ψ_{ch}, ψ_{ph}	Chemical and physical exergy flux (J/mol)
E_a	Apparent activation energy (J/mol)
ex^{ch}	Specific chemical exergy (J/mol)
g	Gibbs free energy (J/mol)
h	Specific enthalpy (J/mol)
R_{gas}	Ideal gas constant (J/(mol K))
s	Specific entropy (J/(mol K))
a_f	Fuel specific chemical exergy (MJ/kg)
LHV	Fuel lower heating value (MJ/kg)
$\mathcal{X}, \dot{\mathcal{X}}$	Exergy in the crank-angle domain (J), (W)
$X, \dot{X}$	Exergy and exergy rate (J), (W)
$S, \dot{S}$	Entropy and entropy rate (J/K), (W/K)
P_{eng}	ICE power (W)
h_{cyl}	Convective heat transfer coefficient (kW/(m^2K))
$\theta, d\theta$	Crank-angle and its differential (rad)
θ_{corr}	Crank-angle correction (rad)
θ_{EC}	Crank-angle at EC (rad)
θ_{SC}	Crank-angle at SC (rad)
θ_{SI}	Crank-angle at SI (rad)
θ_{TDC}	Crank-angle at TDC (rad)
$\Delta\theta$	Combustion duration (rad)
τ_{id}	Ignition delay (rad)
ω_{eng}	ICE rotational speed (rad/s)
T_{eng}	ICE (Nm)

References

[1] J. Tadjdeh, Army driving forward with electric vehicle plans, National Defense 21 (02) (2019).

[2] C. James, T. Y. Kim, R. Jane, A review of exergy based optimization and control, Processes 8 (3) (2020) 364.

[3] A. Gilbert, B. Mesmer, M. D. Watson, Uses of exergy in systems engineering, in: Proceedings of the 2016 Conference on Systems Engineering Research, Mar, 2016, pp. 22–24.

[4] M. D. Watson, System exergy: system integrating physics of launch vehicles and spacecraft, Journal of Spacecraft and Rockets 55 (2) (2018) 451–461.

[5] J. A. Camberos, D. J. Moorhouse, Systems engineering in terms of exergy, International Journal of Aerospace Engineering 2009 (2009).

[6] D. W. Riggins, T. Taylor, D. J. Moorhouse, Methodology for performance analysis of aerospace vehicles using the laws of thermodynamics, Journal of Aircraft 43 (4) (2006) 953–963.

[7] F. Baldi, F. Ahlgren, T.-V. Nguyen, M. Thern, K. Andersson, Energy and exergy analysis of a cruise ship, Energies 11 (10) (2018) 2508.

[8] M. Rosen, D. Scott, Energy and exergy analyses of a nuclear steam power plant (1986).

[9] M. A. Rosen, Energy-and exergy-based comparison of coal-fired and nuclear steam power plants, Exergy, An International Journal 1 (3) (2001) 180–192.

[10] C. Rakopoulos, C. Michos, E. Giakoumis, Availability analysis of a syngas fueled spark ignition engine using a multi-zone combustion model, Energy 33 (9) (2008) 1378–1398.

[11] G. Valencia, A. Fontalvo, Y. Cárdenas, J. Duarte, C. Isaza, Energy and exergy analysis of different exhaust waste heat recovery systems for natural gas engine based on orc, Energies 12 (12) (2019) 2378.

[12] C. Rakopoulos, E. Giakoumis, Second-law analyses applied to internal combustion engines operation, Progress in Energy and Combustion Science 32 (1) (2006) 2 – 47.

[13] A. Alkidas, The application of availability and energy balances to a diesel engine, Journal of Engineering for Gas Turbines and Power 110 (1988) 462–469.

[14] J. H. Van Gerpen, H. N. Shapiro, Second-law analysis of diesel engine combustion (1990).

[15] E. G. Giakoumis, E. C. Andritsakis, Irreversibility production during transient operation of a turbocharged diesel engine, International journal of vehicle design 45 (1-2) (2007) 128–149.

[16] M. Canakci, M. Hosoz, Energy and exergy analyses of a diesel engine fuelled with various biodiesels, Energy Sources, Part B 1 (4) (2006) 379–394.

[17] B. Sayin Kul, A. Kahraman, Energy and exergy analyses of a diesel engine fuelled with biodiesel-diesel blends containing 5% bioethanol, Entropy 18 (11) (2016) 387.

[18] M. Razmara, M. Maasoumy, M. Shahbakhti, R. Robinett, Optimal exergy control of building HVAC system, Applied Energy 156 (2015) 555 – 565.

[19] E. H. Trinklein, G. G. Parker, T. J. McCoy, Modeling, optimization, and control of ship energy systems using exergy methods, Energy 191 (2020) 116542.

[20] E. H. Trinklein, M. D. Cook, G. G. Parker, W. W. Weaver, Exergy optimal multi-physics aircraft microgrid control architecture, International Journal of Electrical Power & Energy Systems 114 (2020) 105403.

[21] M. Razmara, M. Bidarvatan, M. Shahbakhti, R. Robinett, Optimal exergy-based control of internal combustion engines, Applied Energy 183 (2016) 1389 – 1403.

[22] F. Dettù, G. Pozzato, D. M. Rizzo, S. Onori, Exergy-based analysis for hybrid and electric ground vehicles, arXiv preprint arXiv:2103.08145 (2021).

[23] O. Defense, Multi-mission family of vehicles M-ATV, Temecula, CA, USA (2016).

[24] Ford 6.4L Power Stroke, `http://www.powerstrokehub.com/6.4-power-stroke.html`.

[25] Z. Liu, A.-A. M. Mamun, D. M. Rizzo, S. Onori, Combined battery design optimization and energy management of a series hybrid military truck, SAE International Journal of Alternative Powertrains 7 (2) (2018) 155–168.

[26] A.-A. Mamun, Z. Liu, D. M. Rizzo, S. Onori, An integrated design and control optimization framework for hybrid military vehicle using lithium-ion battery and supercapacitor as energy storage devices, IEEE Transactions on Transportation Electrification 5 (1) (2018) 239–251.

[27] P. Lakshminarayanan, Y. V. Aghav, Modelling diesel combustion, Springer Science & Business Media, 2010.

[28] L. Guzzella, C. Onder, Introduction to Modeling and Control of Internal Combustion Engine Systems, Springer, 2010.

[29] A. Widd, P. Tunestål, J. Åkesson, R. Johansson, Single-zone diesel ppc modeling for control, in: 2012 American Control Conference (ACC), IEEE, 2012, pp. 5731–5736.

[30] J. B. Heywood, Internal combustion engine fundamentals, McGraw-Hil, 1988.

[31] C. Rakopoulos, E. Giakoumis, Diesel engine transient operation: principles of operation and simulation analysis, Springer Science & Business Media, 2009.

[32] Z. Žák, M. Emrich, M. Takáts, J. Macek, In-cylinder heat transfer modelling, Journal of Middle European Construction and Design of Cars 14 (3) (2016) 2–10.

[33] P. Punov, N. Milkov, C. Perilhon, P. Podevin, T. Evtimov, Study on the combustion process in a modern diesel engine controlled by pre-injection strategy, in: IOP Conference Series: Materials Science and Engineering, Vol. 252, IOP Publishing, 2017, p. 012090.

[34] A. Bejan, E. Mamut, Thermodynamic optimization of complex energy systems, Vol. 69, Springer Science & Business Media, 1999.

[35] D. Di Battista, D. Vittorini, M. Di Bartolomeo, R. Cipollone, Optimization of the engine intake air temperature through the air conditioning unit, Tech. rep., SAE Technical Paper (2018).

[36] MathWorks, Powertrain blockset, `https://www.mathworks.com/products/powertrain.html`.

[37] U. Asad, M. Zheng, Exhaust gas recirculation for advanced diesel combustion cycles, Applied Energy 123 (2014) 242–252.

[38] R. Sindhu, G. A. P. Rao, K. M. Murthy, Real-time single zone model for simulation of a diesel engine in simulink environment, in: International Conference on Computing, Communication & Automation, IEEE, 2015, pp. 806–811.

[39] A. Sanli, A. N. Ozsezen, I. Kilicaslan, M. Canakci, The influence of engine speed and load on the heat transfer between gases and in-cylinder walls at fired and motored conditions of an idi diesel engine, Applied thermal engineering 28 (11-12) (2008) 1395–1404.

[40] S. Onori, L. Serrao, G. Rizzoni, Hybrid electric vehicles: Energy management strategies, Springer, 2016.

[41] J. A. Camberos, D. J. Moorhouse, Exergy analysis and design optimization for aerospace vehicles and systems, American Institute of Aeronautics and Astronautics, 2011.

[42] I. Prigogine, Introduction to thermodynamics of irreversible processes, New York: Interscience (1967).

[43] I. Dincer, M. A. Rosen, Exergy: energy, environment and sustainable development, Newnes, 2012.